Simulations of Condensed Phase Photochemistry: Cage Effect and Internal Conversion in Azoalkanes and Nitrosamines

Paola Cattaneo, Giovanni Granucci, and Maurizio Persico*

Dipartimento di Chimica e Chimica Industriale Università di Pisa, v. Risorgimento 35, I-56126 Pisa, Italy

Received: September 22, 1998; In Final Form: February 8, 1999

This is a comparative theoretical study of cage effect in the photolysis of two compounds, azomethane and dimethylnitrosamine. Both compounds belong to classes, azoalkanes and nitrosamines, which undergo an almost complete inhibition of photodissociation in condensed phase. We have set up a semiquantitative simulation of the primary photochemical step, based on Langevin dynamics and surface hopping. This required the ab initio determination of quasi-diabatic states and potential energy surfaces (PES). In the PES of both compounds one can identify a region of strong nonadiabatic coupling, marked by the presence of conical intersections, which determines molecular geometry and time of the internal conversion (IC) from S_1 to S_0. Azomethane undergoes a very fast IC when the torsion angle around the N═N bond is about 90°, followed by vibrational energy loss to the solvent: the outcome is isomerization rather than dissociation. On the contrary, the dissociation of nitrosamine takes place essentially in the S_1 potential surface: in this case, the mechanism of cage effect can be described as fast recombination of the fragments, favored by strong nonadiabatic coupling with S_0 at medium-long internuclear distances.

1. Introduction

Several photodissociation reactions, which occur with high quantum yields in the gas phase at low pressures, are inhibited in the condensed phase. This important experimental fact is normally explained in terms of Franck and Rabinovitch's "cage effect":[1] a solvent cage prevents the separation of the fragments, which eventually recombine (see for instance section 3.7 in Wayne's photochemistry textbook[2]). Computer simulations have demonstrated that such a model is adequate, at least in the simple case of I_2 photodissociation.[3,4] The two atoms may even bounce back, after a first hit in the cage walls. According to this picture of the process, the inhibition of photodissociation requires two conditions: one is that, at the time of their recombination, the fragments are in an attractive potential energy surface (PES), normally belonging to the ground electronic state, rather than to the excited state which was populated by photon absorption. The second assumption is that the solvent cage is strong enough as to absorb, without "breaking" or "opening", the vibrational energy excess of the excited solute. Of course, failure in fulfilling one or both of these conditions may explain why photodissociation in solution is not universally inhibited (i.e., not for all solvents, nor for all gas-phase photodissociating solutes).

The efficiency of radiationless transitions depends essentially on the shape of the PES. If the excited and the ground state PES correlate to the same asymptote (as is the case with highly symmetric leaving groups, such as halogen atoms, NO, or linear acyl radicals), the transition may easily take place at fairly large distances between the two fragments. However, many polyatomic molecule undergo "early" internal conversion (IC) at substantially bound geometries, i.e., not far from deep minima in the ground state PES: this requires the presence of funnels, often coinciding with conical intersections.[5−9] An efficient IC helps to fulfill the first condition for the occurrence of a cage effect: it is then interesting to compare IC times with dissociation and caging times; in other words, to discriminate between direct dissociation and electronic predissociation, without discarding intermediate options. After excitation, the reactant is normally endowed with a certain amount of vibrational energy, which may increase sharply as a result of "early" IC. A large fraction of the internal energy of the solute must be spent to escape the ground state potential wells, that is, in breaking chemical bonds. However, vibrational energy can be efficiently transferred to the solvent, thus preventing dissociation: typical times are of the order of tens of picoseconds.[10] Moreover, below a certain energy threshold the reverse IC from ground to excited state will not occur: the solvent effect on radiationless transitions and spectral properties has been studied with both quantum-mechanical and semiclassical methods on a model of photoisomerization.[11,12] We may thus describe the inhibition of photodissociation, focusing on solvent-induced vibrational relaxation (VR) rather than on the "structural" caging concept.

The two pictures of the caging phenomenon, VR and structural, were already clearly expressed at least in 1980, in a study by Hynes et al.,[13] more recently, Wang et al.[3] have discussed their relationship in terms of dissociation and relaxation times. The VR and structural caging descriptions should be taken as limiting cases which bracket a continuum of intermediate descriptions: the energy needed to break the solvent cage is indeed transferred to the solvent, so the two concepts partially merge.[14] However, energy transfer can occur even in the absence of a cage, as in gas phase, where the vibrational quenching of polyatomics may be able to interfere with photochemical processes (although at rates 100−1000 times slower than the collisional rate[15]). Factors such as time and geometry of the IC, transition and dissociation energies, and solvent properties, will determine which model is more appropriate to describe particular systems.

In this paper we investigate the photodissociation of two compounds, azomethane and dimethylnitrosamine, which is

10.1021/jp9838238 CCC: $18.00
Published on Web 04/16/1999

strongly inhibited in solution. To the best of our knowledge, this is the first study of the condensed phase nonadiabatic dynamics for systems of such a complexity, realistically treated with the support of ab initio calculations. We run detailed simulations of the nuclear dynamics and of the electronic radiationless transitions, at a semiclassical level; the dynamical effects of the solvent are introduced by a very simple stochastic model (see section 2). As we shall see, such a model is able to simulate in a semiquantitative way the vibrational relaxation of the solute, but not the structural caging mechanisms. Therefore, the simulations may not reproduce the (almost) complete inhibition of photodissociation which is experimentally observed. For dimethylnitrosamine this is indeed the case, so we may think that structural factors are here important, while the VR effect alone is able to suppress the fragmentation of azomethane. Such a conclusion will be supported by a comparison of other important features of the PES and of the dynamics for the two reactants (sections 3 and 4).

2. Computational Model

Surface Hopping in a Quasi-diabatic Representation. We simulate photochemical reactions by semiclassical dynamics; i.e., we treat the nuclear motion classically and the electronic transitions quantum mechanically. As a nuclear trajectory $\mathbf{R}(t)$ develops, we integrate the time-dependent Schrödinger equation (TDSE) for the electrons:

$$i\hbar \frac{\mathrm{d}|\Psi(t)\rangle}{\mathrm{d}t} = \hat{H}_{\mathrm{el}} |\Psi(t)\rangle \tag{1}$$

The electronic wavefunction $\Psi(t)$ is expanded over a set of quasi-diabatic[16,17] states $\{|\eta_1\rangle, \ldots |\eta_N\rangle\}$.

$$|\Psi(t)\rangle = \sum_I D_I(t)\, \mathrm{e}^{-i/\hbar \int_0^t H_{\mathrm{II}}(\mathbf{R}(t'))\mathrm{d}t'} |\eta_I(\mathbf{R}(t))\rangle \tag{2}$$

The $|\eta_I\rangle$ are defined so as to minimize the dynamical couplings $\langle\eta_I|\partial/\partial R_\alpha|\eta_J\rangle$, and their determination by initio calculations follows a method based on diabatic templates, originally proposed by one of us[18,19] and recently extended to treat the case of several reaction coordinates.[20] The **H** matrix represents the electronic hamiltonian in the quasi-diabatic basis. Its matrix elements $H_{IJ} = \langle\eta_I|\hat{H}_{\mathrm{el}}|\eta_J\rangle$ are expressed as analytical functions of the internal nuclear coordinates, fitting the ab initio values.

Through the expansion (2), the TDSE takes the form of a set of coupled equations:

$$\frac{\mathrm{d}D_I}{\mathrm{d}t} = -\frac{i}{\hbar} \sum_{J(\neq I)} D_J(t)\, H_{IJ}(\mathbf{R}(t))\, \mathrm{e}^{i\phi_{IJ}(t)} \tag{3}$$

with $\phi_{IJ} = (1/\hbar)\int_0^t (H_{II} - H_{JJ})\, \mathrm{d}t'$. The $D_I(t)$ coefficients are determined by an efficient numerical algorithm.[21]

The eigenvalues of **H** are the adiabatic energies $E_K(\mathbf{R})$; its eigenvectors $\mathbf{T}_K$ represent the adiabatic wave functions $|14_K\rangle$ in the diabatic basis.

$$\mathbf{H}\mathbf{T}_K = E_K \mathbf{T}_K \tag{4}$$

$$|\psi_{\mathrm{K}}\rangle = \sum_I T_{IK} |\eta_I\rangle \tag{5}$$

The transformation matrix **T** connects the adiabatic probabilities P_K to the diabatic coefficients of the development (2):

$$P_K(t) = |\langle\Psi(t)|\psi_K\rangle|^2 = \sum_{I,J} D_I^* D_J\, e^{i\phi_{IJ}} T_{IK} T_{JK} \tag{6}$$

A trajectory is run on a given adiabatic surface $E_K(\mathbf{R})$ and may hop to another one, according to variations in the P_K probabilities; Tully's "fewest switches" prescription for surface hopping[22,23] is applied. After the electronic transition, the kinetic energy is readjusted so as to conserve the total energy. More details about the trajectory surface hopping (TSH) model, although in slightly different versions, can be found in our previous work.[24,25]

Langevin Dynamics. It will be noticed that all the information concerning the reacting molecule and required to run both the nuclear and the electronic dynamics is contained in the **H** matrix. The influence of the solvent on the nuclear motion is introduced at the simplest level, by integrating Langevin's equation:

$$\dot{P}_\alpha = -\gamma_\alpha P_\alpha - \frac{\partial E_K(\mathbf{R})}{\partial R_\alpha} + X_\alpha(t) \tag{7}$$

where $P_\alpha = m_\alpha \dot{R}_\alpha$ is the conjugated moment of the R_α coordinate and m_α the associated mass. $X_\alpha(t)$ is a Gaussian random white noise, with the properties $\langle X_\alpha\rangle = 0$, $\langle \mathrm{X}_\alpha(0) X_\beta(t)\rangle = 2m_\alpha\gamma_\alpha kT\delta_{\alpha\beta}\delta(t)$. The numerical implementation of eq 7 follows van Gunsteren and Berendsen.[26] The solution of eqs 3, the surface-hopping algorithm, and the stochastic simulation of solvent effects have all been introduced as variants of the VENUS classical trajectory program, by Hase and co-workers.[27] The resulting computational model will be hereafter called LSH (Langevin surface hopping).

The LSH model contains a set of arbitrary constants, the friction coefficients γ_α. As the escape of photodissociated fragments from the solvent cage is essentially a diffusional process, one may think that the γ_α should be chosen so as to reproduce the experimental diffusion coefficients for the fragments themselves, or at least for related molecules. We apply a generalization of Einstein's equation

$$D = kT \Big/ \sum_\alpha \gamma_\alpha m_\alpha \tag{8}$$

to relate the molecular diffusion coefficients D and the atomic γ_α's. However, it is well-known that the Langevin approach with diffusional friction coefficients overestimates the vibrational relaxation rates.[28] In fact, the γ_α coefficients should be time dependent, with decreasing Fourier components in the high-frequency domain. Such a generalized Langevin approach has been applied with some success[28,29] to the vibrational relaxation of I_2, but its extension to polyatomics would introduce a rather complex set of parameters to describe the solute−solvent energy transfer. As we shall see in the following, with a suitable choice of the friction coefficients the LSH model may yield a semiquantitative treatment of the photochemical dynamics in the condensed phase, provided that structural solvent effects are not too important.

3. Azomethane

Acyclic azoalkanes photodissociate in low-pressure gas phase, when excited in the n → π^* (S_1) band, according to

$$\mathrm{R{-}N{=}N{-}R'} \xrightarrow{h\nu} \mathrm{N_2} + \mathrm{R^\bullet} + \mathrm{R'^\bullet} \tag{9}$$

with quantum yields close to 1. One of the best studied examples is *trans*-azoisopropane.[30] Its photodissociation is partially suppressed in the presence of a buffer gas: with CO_2 at rather high

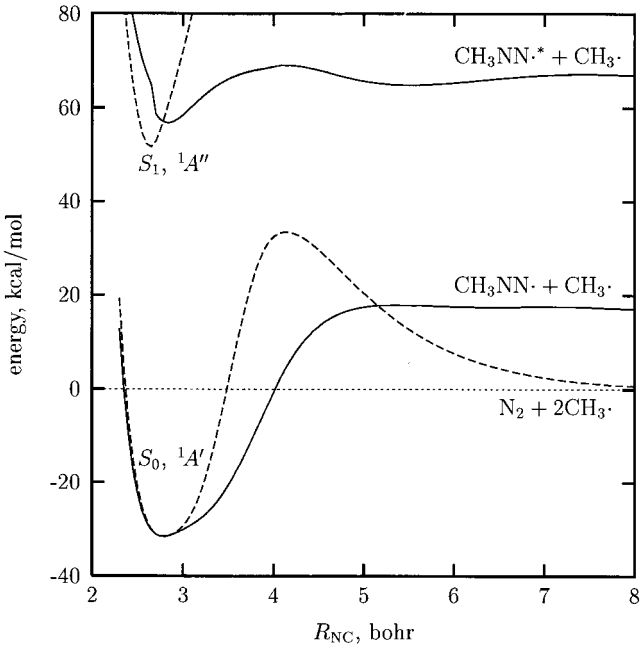

Figure 1. Potential energy curves for the dissociation of *trans*-azomethane. Full curves: breaking of one N−C bond, S_0 and S_1 energies as functions of $R_{N_1C_1}$; dashed curves, symmetric breaking of both N−C bonds, energies as functions of $R_{N_1C_1} = R_{N_2C_2}$. All other coordinates optimized in the S_0 PES.

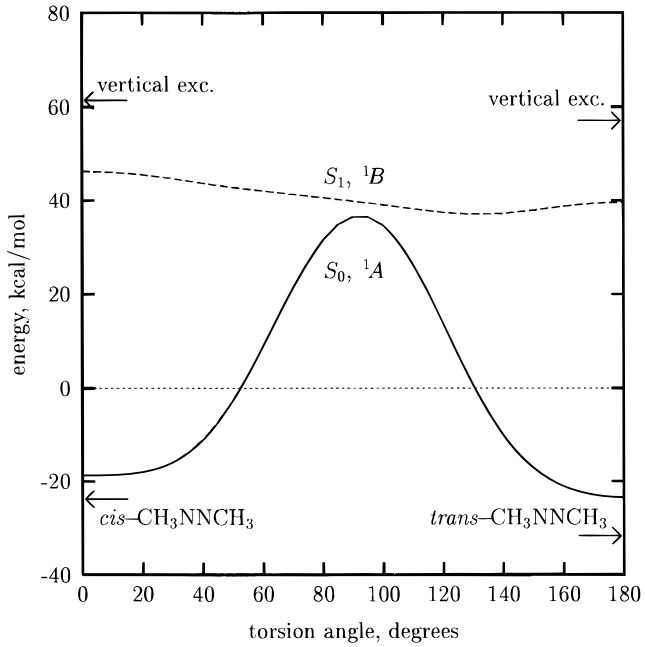

Figure 2. Potential energy curves for the torsion of the N═N bond of azomethane. S_0 and S_1 energies as functions of the CNNC dihedral angle. All other coordinates optimized in the S_1 PES. Arrows indicate the cis and trans minima in S_0 and the corresponding vertical excitation energies.

pressures (1 atm or more), the quantum yield $\Phi_{trans\rightarrow dissoc}$ decreases to about 0.3 when irradiated with $\lambda = 334$ nm, and to 0.5 with $\lambda = 313$ nm; starting with the cis isomer, one obtaines higher yields. Insofar as dissociation is inhibited, the geometrical isomerization is observed, with cis to trans conversion much easier than trans to cis: $\Phi_{cis\rightarrow trans}$ can be as high as $\simeq$0.5, while $\Phi_{trans\rightarrow cis}$ does not exceed 0.15 in the high-pressure limit. Recent experimental studies on the photolysis of azomethane ($R^\bullet = R'^\bullet = CH_3^\bullet$) have focused on the timing of the breaking of the two N−C bonds: some authors conclude in favor of a stepwise dissociation[31,32]

$$\text{trans}-CH_3NNCH_3 \xrightarrow{h\nu} CH_3NN^\bullet + CH_3^\bullet \qquad (10)$$

$$CH_3NN^\bullet \rightarrow N_2 + CH_3^\bullet \qquad (11)$$

while others interpret their results in terms of unsymmetrical but almost simultaneous dissociation.[33,34] Our TSH simulations on the photodissociation of isolated azomethane support the latter conclusion.[35,36]

In the condensed phase the photodissociation is almost completely inhibited (see Engel's review[37] and references therein). For *trans*-azomethane at $\lambda = 365$ nm we have $\Phi_{trans\rightarrow dissoc} = 0.17$ in i−octane, 0.09 in benzene, and 0.01 in water. In benzene the two isomerization quantum yields are almost equal: $\Phi_{trans\rightarrow cis} = 0.42$, $\Phi_{cis\rightarrow trans} = 0.45$.

A. Potential Energy Surfaces. We have run LSH simulations of azomethane photochemistry, based on a quasi-diabatic ab initio Hamiltonian **H**, corrected to take into account the available experimental data (mainly the dissociation energy to $N_2 + 2CH_3^\bullet$). We have also incorporated the zero-point energy in the diagonal matrix elements, in order to make up for its neglect in classical dynamics. Details of the calculations and of the fitting procedure will be described elsewhere.[38,39] Overall, our results are in agreement with those of Liu et al.[40]

In Figure 1 we show the potential energy profiles for the dissociation of *trans*-azomethane. All energies are given relative to the dissociation products $N_2 + 2CH_3^\bullet$. Two pathways have been considered: breaking of one N−C bond, leading to $CH_3NN^\bullet + CH_3^\bullet$, and symmetric breaking of both N−C bonds, with $R_{N_1C_1} = R_{N_2C_2}$. In both cases all other coordinates have been optimized for the ground state PES: the excited state energies are computed at the same geometries. Notice that at planar geometries the quasi-diabatic PES, H_{II}, and the adiabatic ones, E_K, coincide because S_0 and S_1 belong to different symmetries, $^1A'$ and $^1A''$, respectively. The one-bond dissociation curve shows no barrier in the ground state, but leads to products of higher energy in comparison with the symmetric bond breaking. In fact, $CH_3NN^\bullet$ is unstable with respect to $N_2 + CH_3^\bullet$ by 16.8 kcal/mol, and the activation energy for its dissociation is only 11.0 kcal/mol (27.8 kcal/mol higher than the products). The symmetric bond breaking requires an activation energy of 65.1 kcal/mol in S_0, while in S_1 it leads to a high-energy excited state of N_2, not accessible photochemically at the usual wavelengths.

In Figure 2 we show the isomerization potential energy curves: here the leading coordinate is the CNNC dihedral angle, and all other coordinates have been optimized in the S_1 PES. Again, the quasi-diabatic and adiabatic PES coincide, because of symmetry (C_2 group). The trans isomer is found at −31.6 kcal/mol (with respect to the dissociation products) and the cis one at −23.7 kcal/mol. S_1 has a shallow minimum at CNNC $\simeq$ 130° (37.1 kcal/mol). At CNNC $\simeq$ 90° the S_0 and S_1 curves are very close and, with slight geometrical distortions (without symmetry breaking) they do cross. The lowest point of the crossing seam is at 40.5 kcal/mol, i.e., 72.1 kcal/mol over the trans minimum and well below the vertical excitation energy (88.6 kcal/mol). Strong nonadiabatic interactions, able to promote a fast IC, are present also along the minimum energy path in S_1, which runs close to the crossing seam without going through it.

B. Langevin Nonadiabatic Dynamics. The friction coefficients for the LSH calculations have been chosen so as to reproduce certain molecular diffusion coefficients D in water[41]

at 25 °C. The photofragments of interest here are N_2, $CH_3^\bullet$ and $CH_3NN^\bullet$, and in the next section (nitrosamine photodissociation), $(CH_3)_2N^\bullet$, and NO. Of these, only $D[N_2]$ is known, so we have assumed $D[NO] = D[N_2]$ and $\gamma_O = \gamma_N$, which yields $\gamma_N = 35.5\ ps^{-1}$: this value has been used for the azomethane fragmentation as well. In place of $D[(CH_3)_2N^\bullet]$ we have taken $D[(CH_3)_2CO]$ (a molecule with a similar structure), and we have deduced γ_H and γ_N with the assumption that they are equal to each other and that $\gamma_C = 0$ (in all cases, the C atom has the weakest interaction with the solvent). Then, for the $(CH_3)_2N^\bullet$ fragment we get $\gamma_H = \gamma_N = 97.4\ ps^{-1}$. The same values have been applied also to azomethane.

In order to reduce the VR rates to realistic values, we have multiplied all the γ_α by a factor $F_\gamma \leq 1$, and run several simulations with different F_γ values. Each simulation consisted of a batch of 500 trajectories. The initial conditions have been sampled by running Langevin dynamics in the ground state for several picoseconds, starting with the trans or the cis equilibrium geometry; then, at intervals of 20 fs, a Franck−Condon excitation (adiabatic surface switch without changing nuclear coordinates and momenta) starts a new trajectory. The trajectory is stopped when both NC bond lengths exceed 8 bohr (dissociation) or when the total energy falls below 5 kcal/mol (IC to ground state azomethane with or without isomerization). However, very few trajectories complete the dissociation of both N−C bonds within 100 ps, the maximum allowed time for each run: more frequently, only one bond is broken with formation of the transient species $CH_3NN^\bullet$.

It is interesting to compare the LSH results with those of TSH calculations for the photolysis of the isolated molecule[35,36] and with molecular dynamics (MD) simulations.[42] The latter combine classical MD trajectories for the reactant surrounded by 120 water molecules with the surface-hopping algorithm. Periodic boundary conditions and standard potentials for the solute−solvent interactions were used, while the internal potentials for azomethane were the same as in the present work. In all three cases the first act is torsion around the N=N bond in the S_1 surface, followed by transition to S_0 when CNNC = 70°−110°. The average time of the first surface hopping of each trajectory, $\bar{t}_{SH}$, is substantially influenced by the solvent only when large friction coefficients are applied ($F_\gamma > 0.1$), because then the torsional motion is slowed down. We get $\bar{t}_{SH} = 323$ fs in vacuo[36] and $\bar{t}_{SH} = 396$ fs with MD simulations; comparable values are found with the LSH method, for $F_\gamma \leq 0.1$ (see Table 1). Once in S_0, the energy transfer to the solvent and to internal coordinates other than torsion cooperate in removing the solute molecule from the strong nonadiabatic interaction region, thus reducing the probability of backward hoppings. The S_1 population as a function of time is shown in Figure 3. The decay starts after an induction time of about 80 fs, corresponding to half an oscillation of the torsional coordinate. The time dependence is similar in vacuo and for the lowest range of friction coefficients. The two solvent effects seen above (slower dynamics in the S_1 PES and decreased probability of backward transitions) influence the IC rate in opposite ways, and partially cancel each other.

The VR rates of course depend on the friction coefficients and also on the region of the PES where the trajectory is evolving. We have evaluated the first-order decay rate of the internal energy of azomethane, by applying at each time step Δt the equation

$$\Delta E = -K[E(t) - E(\infty)]\Delta t \qquad (12)$$

Here $E(t)$ is the potential plus kinetic energy of the nuclei and

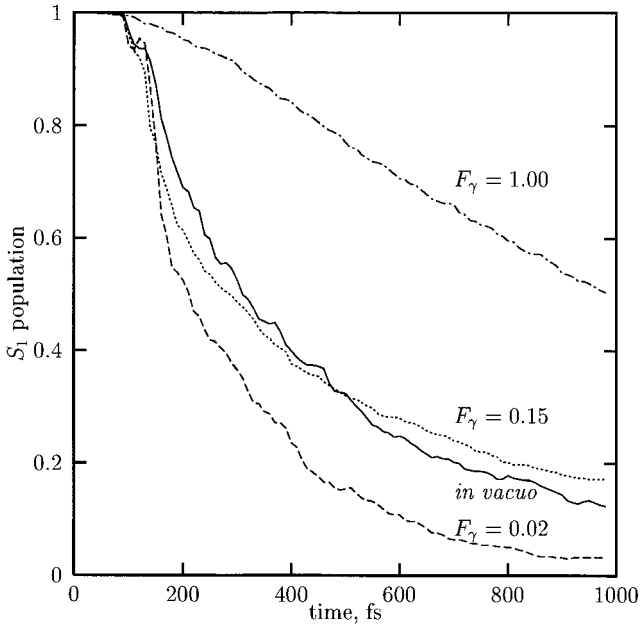

Figure 3. S_1 populations as functions of time in TSH (in vacuo) and LSH simulations (with three different friction coefficients factors $F\gamma$).

TABLE 1: First Surface Hopping Time Averaged over All Trajectories ($\bar{t}_{SH}$) and Vibrational Relaxation Rate Constants ($\bar{K}$) of Azomethane, as Functions of the Friction Coefficients Factor F_γ

		$\bar{K}$, ps^{-1}		
F_γ	$\bar{t}_{SH}$, fs	cis-azomethane	trans-azomethane	$CH_3NN^\bullet + CH_3^\bullet$
0.02	304	1.28	1.21	1.13
0.03	329	1.83	1.75	
0.05	329	2.77	2.71	
0.10	422	5.34	4.94	
0.15	578	6.74	6.33	
0.20	728	8.37	7.95	
0.30	779	10.10	8.61	
0.50	982			
1.00	999			

$E(\infty)$ is its long-time average. $E(\infty)$ depends on the relative minimum where the trajectory is eventually trapped and is obtained in separate runs in the S_0 PES. We average the K values obtained from eq 12 over time and trajectories, separately for cisoid, transoid, and dissociated ($CH_3NN^\bullet + CH_3^\bullet$) geometries: the $\bar{K}$ values we obtain are rather similar in the three cases (see Table 1), the essential differences being taken into account by the final energies $E(\infty)$. The same procedure, applied to our MD simulations, yields $\bar{K} \simeq 0.42-0.45\ ps^{-1}$. This is an indication that a friction coefficient factor $F_\gamma = 0.02$ or even smaller is a reasonable choice.

Figure 4 shows the dependence of the quantum yields on the friction factor F_γ. In computing the photodissociation quantum yields we have counted trajectories which break either one or two N-C bonds, without distinction. With large friction coefficients, the photodissociation is almost completely inhibited and the trans-cis isomerization quantum yields are also very low: the VR is so fast that most trajectories do not proceed much further than the minimum in S_1 (CNNC ≃ 130°), so that the IC to S_0 occurs at transoid geometries. In this case, the computed $\Phi_{trans\rightarrow cis}$ quantum yield is too small. A fair agreement with the experimental findings is obtained with much smaller friction coefficients ($F_\gamma = 0.02 \div 0.05$): we have $\Phi_{cis\rightarrow trans}$ slightly larger than $\Phi_{trans\rightarrow cis}$, both in the range $0.3 \div 0.5$; $\Phi_{trans\rightarrow dissoc} < 0.1$ and $\Phi_{cis\rightarrow dissoc}$ substantially larger than $\Phi_{trans\rightarrow dissoc}$. Because the cis isomer has also a more intense n

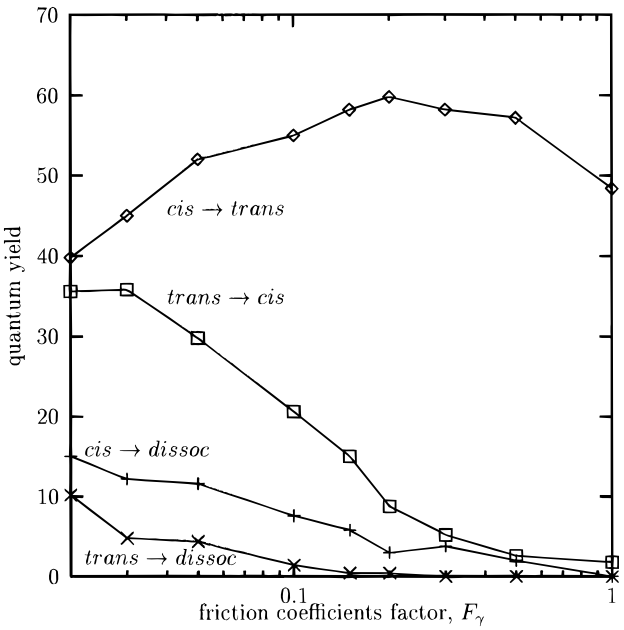

Figure 4. Quantum yields for *cis*- and *trans*-azomethane photolysis according to LSH simulations, as functions of the factor F_γ multiplying the friction coefficients.

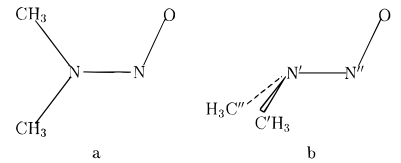

Figure 5. (a) Equilibrium geometry for S_0 of dimethylnitrosamine; (b) pyramidalized and twisted geometry.

$\rightarrow \pi^*$ absorption band, indirect photodissociation with preliminary trans $\rightarrow$ cis conversion may be an important route for many trans-azoalkanes.

4. Dimethylnitrosamine

The nitrosamines in the gas phase undergo dissociation of the N−N bond after excitation in the n $\rightarrow \pi^*$ band (S_1 state):

$$\mathrm{RR'N{-}NO} \xrightarrow{h\nu} \mathrm{RR'N^\bullet} + \mathrm{NO^\bullet} \qquad (13)$$

The reaction mechanism for dimethylnitrosamine, $(CH_3)_2N-NO$, has been investigated in crossed beam experiments, by correlating the recoil velocity of the fragments and the angular momentum of NO with the polarization of the pump light pulse.[43,44] Ab initio and classical trajectory studies by our group[45,46] have shown that the molecule undergoes an important geometry rearrangement in the excited state prior to dissociation. The preferred conformation in S_0 is planar (see Figure 5a), while in S_1 the aminic N atom is pyramidalized and the N−N bond is rotated by 90° (Figure 5b). If planarity is imposed, a potential barrier of about 20 kcal/mol prevents dissociation in S_1: therefore, the molecule converts to the twisted and pyramidalized conformation, where no activation energy is required to dissociate. These findings have been confirmed shortly afterwards by resonance Raman spectroscopy.[47]

The photodissociation is strongly inhibited in condensed phase,[48] although there is some evidence of the production (and fast recombination) of the $(CH_3)_2N^\bullet$ and $NO^\bullet$ radicals.[49] In order to investigate this phenomenon we have performed LSH simulations, using a two-state quasi diabatic ab initio Hamiltonian **H**.

A. Potential Energy Surfaces. The ab initio calculations were run in the framework of the CIPSI algorithm.[50,51] The atomic basis set used was the PS−31G* of Bouteiller et al.[52] As the methyl groups are relatively unaffected by the excitation and dissociation processes, we have eliminated the d polarization functions of the carbon atoms. The MO's used in the CIPSI procedure were the natural orbitals of state-averaged CASSCF calculations for S_0 and S_1, performed including in the active space 12 electrons and 8 MO; the active MO's correlate at dissociation with the two lone pairs and the degenerate π and π^* MO's of NO, and with the lone pair and the p orbital of the N atom of $(CH_3)_2N^\bullet$ (see the orbital correlation scheme of ref 46). The CIPSI calculations involved, at each geometry, four steps of perturbation and configuration selection,[51] with the selection thresholds $\eta = 0.05$, 0.03, 0.02, and 0.007. The fifth and last step involved the determination of variational wave functions expanded over up to 10^4 Slater determinants. In the perturbation step, single and double excitations were generated from a subspace including 3500−4000 determinants, selected with a threshold $\eta_G = 0.009$.

As long as the N−N−O plane is a symmetry element, for both conformations of Figure 5, a and b, S_0 is $^1A'$ and S_1 is $^1A''$. However, around $R_{NN} = 5$ bohr in the twisted and pyramidalized conformation the energy ordering of the two symmetry states changes and $^1A''$ is lower at larger distances. Therefore, a conical intersection lies right in the minimum energy path for dissociation, at moderately large fragment separation. We have defined two quasi-diabatic states with the method of diabatic templates,[18,19] in such a way that $|\eta_1\rangle$ keeps the character of the $^1A'$ state, and $|\eta_2\rangle$ that of $^1A''$, even at nonsymmetric geometries.

The quasi diabatic hamiltonian matrix **H** has been fitted using two different analytic functions of nine skeletal coordinates (see Figure 5b): R_{NN}, R_{NO}, R_{NC}, and $R_{NC''}$ are bond lengths; $\gamma \equiv$ N′N″O, $\phi_1 \equiv$ C′N′N″, and $\phi_2 \equiv$ C″N′N″ are bond angles; $\delta_1 \equiv$ C′N′N″O and $\delta_2 \equiv$ C″N′N″O are dihedral angles. We have also used four other coordinates (that can be expressed as functions of the preceding ones): $\beta \equiv$ C′N′C″ bond angle; $\eta \equiv$ AN′N″ pyramidalization angle (A being a point on the bisector of β); $\theta \equiv$ AN′N″O dihedral angle, torsion around the N−N axis; $\alpha \equiv$ C′N′N″A dihedral angle, torsion around the bisector of β. The diagonal elements of **H** have been fitted with an analytic function:

$$H_{II} = U_{II}^{\mathrm{ske}} + U^{\mathrm{met}} \qquad (14)$$

where U^{met} is a function of the internal coordinates of the methyl groups and U_{II}^{ske} depends only on the nine skeletal coordinates. U^{ske} is a sum of terms, in such a way that each of the nine coordinates is coupled at least to R_{NN}, that is, the most important coordinate in the dissociation process:

$$U^{\mathrm{ske}} = U_0(R_{NN}) + U_{NO}(R_{NN},R_{NO}) + U_{NC}(R_{NN},R_{NC'}) + U_{NC}(R_{NN},R_{NC''}) + U_{CNC}(R_{NN},\beta) + U_{ANG}(R_{NN},\phi_1,\phi_2,\gamma,\delta_1,\delta_2) \qquad (15)$$

The above terms are defined by a set of 18 parameters A_i, obviously different for H_{11} and H_{22}, which are in turn functions of R_{NN}:

$$U_0 = A_1$$

$$U_{NO} = A_2(R_{NO} - A_3)^2/2$$

$$U_{NC} = A_4(R_{NC} - A_5)^2/2 \quad (16)$$

$$U_{CNC} = A_6(\beta - A_7)^2/2$$

The term U_{ANG}, which depends on the relative orientation of the two fragments $(CH_3)_2N^{\bullet}$ and NO, is built so as to obey the appropriate symmetry restrictions and to allow a sufficient flexibility in the fitting:

$$U_{ANG} = A_8[(\phi_1 - A_9)^2 + (\phi_2 - A_9)^2]/2 + A_{10}\cos\gamma + A_{11}\cos 2\gamma + A_{12}\cos 3\gamma + A_{13}\cos\eta + A_{14}\cos 2\eta + A_{15}\cos 3\eta + A_{16}\sin\gamma\,(\cos\delta_1\sin\phi_1 + \cos\delta_2\sin\phi_2) + A_{17}\sin^2\gamma\,(\cos 2\delta_1\sin^2\phi_1 + \cos 2\delta_2\sin^2\phi_2) + A_{18}\sin\gamma\,(\cos 3\delta_1\sin\phi_1 + \cos 3\delta_2\sin\phi_2) \quad (17)$$

The methyl contribution U^{met} is the same as in ref 46, with the exception of the value of the threefold barrier for methyl torsion (1.163 instead of 1.722 kcal/mol).

For the conformations with C_s symmetry the off diagonal part H_{12} is zero, as the two states belong to different irreps. Moreover, $H_{12} \rightarrow 0$ when $R_{NN} \rightarrow \infty$. Therefore, H_{12} has to depend on the angles α and θ that specify the relative orientation of the two fragments, on R_{NN} and on the two bond lengths $R_{NC'}$ and $R_{NC''}$. That last dependence has been neglected, because the methyl groups are relatively unaffected by the dissociation process. We found it convenient to express H_{12} as a function of R_{NN} and of the angles ϕ_1, ϕ_2, δ_1, δ_2, θ, and η:

$$H_{12} = B_1\sin(\phi_1 - \phi_2)\sin(\delta_1 - \delta_2) + B_2\sin(\phi_1 - \phi_2)\cos(\phi_1 - \phi_2)\sin(\delta_1 - \delta_2) + B_3\sin(\phi_1 - \phi_2)\cos 2(\phi_1 - \phi_2)\sin(\delta_1 - \delta_2) + B_4\sin\eta\sin\theta + B_5\sin^2\eta\sin\theta + B_6\sin^2\eta\sin\theta\cos\theta + B_7\sin^2\eta\sin\theta\cos 2\theta \quad (18)$$

The dependence of H_{12} on R_{NN} is contained in the B_i parameters, that play the same role as the A_i for H_{II}.

As we are interested only in the behavior of the system at medium to large N−N separations, the ab initio calculations were run for $R_{NN} = 4.0$, 4.5, 5.0, 5.5, 5.9, 7.0 bohr, and ∞. For each of these R_{NN} values, a reference geometry was determined by performing a CASSCF optimization for the S_1 state, imposing the twisted and pyramidalized conformation of Figure 5b. Then, the CIPSI calculations were done for geometries obtained varying, independently or simultaneously, the coordinates $R_{NC'} = R_{NC''}$, R_{NO}, β, γ, α, and θ, for a total of 130 points. The parameters A_i and B_i were determined for each R_{NN} value, fitting the ab initio points with the functions defined above; the overall variance of the fitting was, in kcal/mol, 0.69 for H_{11}, 0.52 for H_{22}, and 0.41 for H_{12}. Finally, all of the $A_1...A_{18}$, $B_1...B_7$ parameters were interpolated as functions of R_{NN} with cubic splines.[39]

The minimum energy profiles for the N−N bond breaking in the two PES here considered are shown in Figure 6. At each point, all the coordinates except R_{NN} were optimized, with the restriction of keeping the pyramidalized and twisted conformation of Figure 5b. The PES were continued for $R_{NN} < 4$ bohr according to our previous results.[46] At the planar equilibrium geometry in S_0 the R_{NN} distance is about 2.6 bohr. After photoexcitation with $\lambda = 363.5$ nm the system has about 34 kcal/mol in excess with respect to the dissociated fragments.[43,46] In the pyramidalized and twisted conformation (Figure 5b) there is almost no barrier toward the dissociation. At medium to large

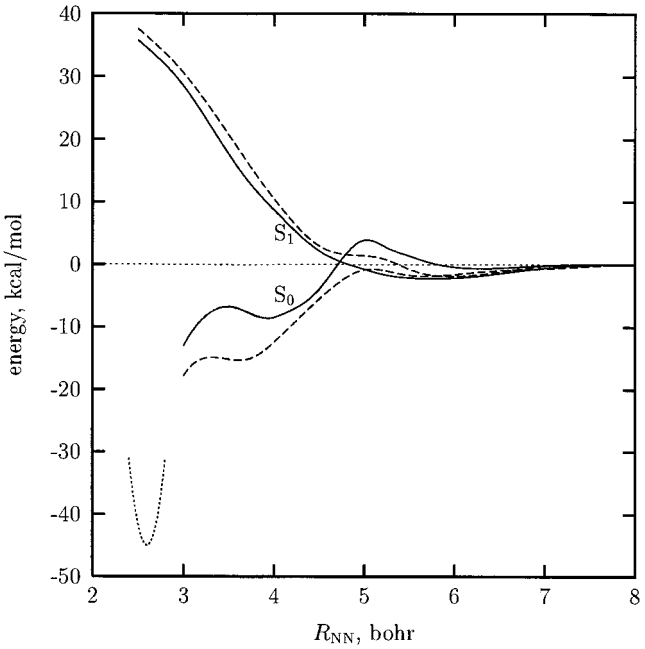

Figure 6. Potential energy curves of dimethylnitrosamine, as functions of R_{NN}. All other coordinates are optimized. Full lines: S_1 is optimized, twisted, and pyramidalized conformation (Figure 5b). Dashed lines: S_0 is optimized (same conformation). Dotted lines: S_0 is optimized (planar conformation, Figure 5a).

R_{NN} distance, three features of the PES are relevant. The conical intersection between S_0 and S_1 occurs at $R_{NN} \simeq 4.7$ bohr along the minimum energy path in S_1, at a potential energy almost equal to that of the dissociated fragments. In S_1 we find a shallow minimum, more pronounced than in S_0: its depth is about 2.3 kcal/mol, at $R_{NN} \simeq 5.8$ bohr. In the S_0 PES there is almost no barrier to the recombination of the two fragments (Figure 6, dashed curve).

B. Langevin Nonadiabatic Dynamics. In order to study the dynamics in solution we have used the LSH method, with the same friction coefficients as in the case of azomethane with $F_\gamma = 1$. This corresponds to diffusional motion in H_2O; we have obtained qualitatively similar results considering CCl_4 as solvent, that is, decreasing the γ_α's by about 30%.

We selected the initial conditions assuming classical Boltzmann distribution for all the internal and rotational coordinates, with the exception of R_{NN}. The sampling was performed by running Langevin dynamics on the S_1 PES with R_{NN} fixed at 2.6 bohr over a time (3 ps) sufficient to obtain the equipartition value for the averaged kinetic energy and a random distribution of the vibrational energy among the internal coordinates. This corresponds to the assumption that the slow conversion from conformation 5a to 5b in the S_1 PES is accompanied by full thermalization due to solute−solvent interactions. At regular time intervals the constraint on R_{NN} is released and a new reactive trajectory is started. The integration was stopped following one of the three conditions: (a) time of the reactive trajectory exceeding 5 ps; (b) $R_{NN} > 10$ bohr (dissociation); (c) potential energy with respect to the dissociation limit < -9 kcal/mol (recombination).

The results are shown in Figure 7. The system passes through the crossing seam at $R_{NN} \simeq 4.7$ bohr within the first 100 fs. This causes a depletion of S_1 by about 50% and, in the following 200 fs, a steep raising of the fraction of recombined trajectories that reaches 15%. The existence of a conical intersection along the reaction path plays therefore an important role; however, even in conjunction with a generic mechanism of solute−solvent energy transfer, it is not suffucient to account for the inhibition

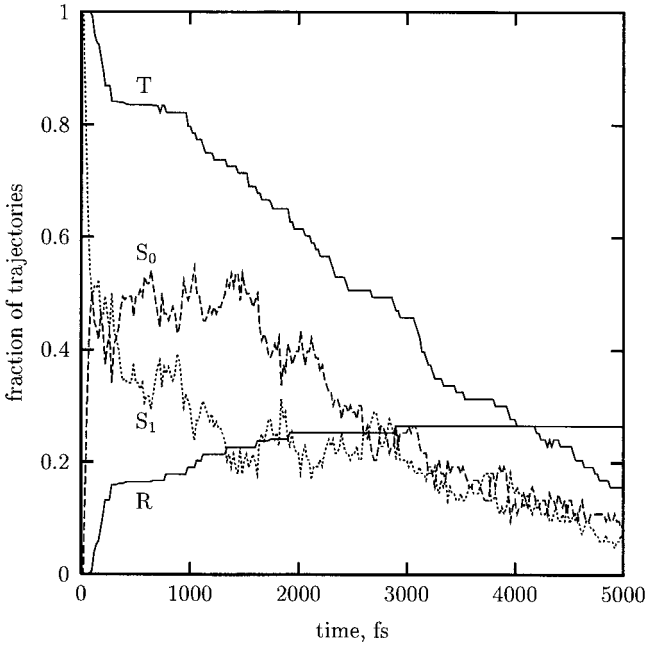

Figure 7. LSH time-dependent results for dimethylnitrosamine in H_2O. R curve: recombined trajectories (fraction of trajectories that have reached the recombination condition). S_0 and S_1 curves: state populations, excluding recombined and dissociated trajectories. T curve: total $S_0 + S_1$ (trajectories still running at time t).

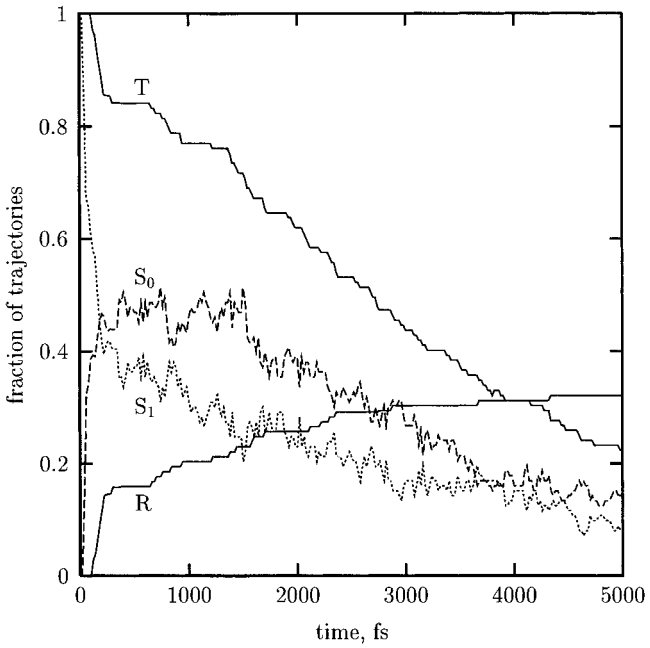

Figure 8. As in Figure 7, but with the PES modified by adding the cavitation energy.

of photodissociation. The trajectories still running for $t > 300$ fs are mainly confined in the flat region of the PES with large R_{NN}. In this region the leading mechanism for the recombination should be the structural caging, which is quite underestimated by the LSH method, as the fraction of the recombined trajectories reaches only 25% after 5 ps. Such a behavior is not unexpected: the Langevin approach cannot reproduce the strong directionality of the solute−solvent collisions (more likely to shorten the interfragment separation than to lengthen it) and the binding properties of the solute molecules, which are the main aspects of the structural caging mechanism.

A partial account of structural solvent effects on changes of solute geometry may be given by evaluating the cavitation free energy (ΔG_{cav}). This is the energy employed to form a cavity in the solvent having appropriate shape and size to fit the solute. In order to take into account the effect of cavitation on the photodissociation dynamics, we have added ΔG_{cav} to our PES. For the evaluation of ΔG_{cav} we have used the Pierotti−Claverie formula[53] that only involves geometrical parameters of the solute (van der Waals radii of the atoms) and the solvent (molecular radii). The cavitation energy grows with the distance R_{NN} until an asymptotic value is reached when two separate cavities are formed. It is therefore an attractive term that should oppose dissociation and favor recombination. We have only considered the variation of ΔG_{cav} with R_{NN}, so H_{11} and H_{22} have been modified by adding $\Delta G_{cav}(R_{NN})$ to U_0 in eq 16. The deformation of the PES is modest: −1.38 kcal/mol at $R_{NN} = 4$ bohr and −0.57 kcal/mol at $R_{NN} = 5$ bohr. The results of the simulation are shown in Figure 8. The inclusion of ΔG_{cav} introduces only slight modifications in the dynamics: the number of recombined trajectories increases by about 5% with respect to Figure 7. Apparently, cavitation, according to the continuous equilibrium representation we have applied, plays only a modest role in the caging mechanism.

5. Conclusions

In this paper, we have studied two examples of cage effect by semiclassical simulations. The PES and electronic couplings were accurately determined by ab inito theory, and the semiclassical surface hopping treatment is probably the best one can do for polyatomics with large-amplitude nonharmonic motions along several coordinates. On the other hand, the representation of solvent effects was done at the simplest possible level, by integrating Langevin's equation (LSH model). In practice, the solvent acts as a thermal bath, with a solute−solvent coupling which can be modulated through the friction coefficients.

The results are qualitatively different in the two cases. For azomethane, we obtain a fair agreement with the experimental results; in particular, the photodissociation is strongly inhibited in our simulations. The success of the LSH model shows that the vibrational relaxation of the solute due to energy exchange with the solvent is the basic mechanism of the cage effect. This is due to a very efficient IC, faster than the bond-breaking process: once in the S_0 PES, where dissociation should take place, the excess vibrational energy is rapidly transferred to the solvent.

In the case of nitrosamine, the $S_1 \rightarrow S_0$ radiationless transition takes place at rather large internuclear distances and at energies close to the dissociation limit: the presence of a conical intersection is important but probably not essential under this respect. In the almost flat long-range part of the potential, caging is mostly due to "structural" effects, i.e., the directionality of solute−solvent collisions and the strength of the cage walls. These aspects cannot be taken into account by the LSH model, and its partial failure is an indirect indication of their importance.

More insight on the caging mechanism will come out of molecular dynamics simulations including explicitly an adequate number of solvent molecules. We feel, however, that the present results illustrate in a convincing way two types of caging, one based on solvent-induced vibrational relaxation and the other one on structural solvent effects: the factors which determine their relative importance (shape of the PES, IC rate, and geometry where the IC takes place) are also clear.

Acknowledgment. This work was supported by grants of the Italian MURST and by the CNR project "Dynamics, reactivity and structure of molecular solutes".

References and Notes

(1) Franck, J.; Rabinowitch, E. *Trans. Faraday Soc.* **1934**, *30*, 120.
(2) Wayne, R. P. *Principles and applications of photochemistry*; Oxford S. P.: Oxford, UK, 1989.
(3) Wang, W.; Nelson, K. A.; Xiao, L.; Coker, D. F. *J. Chem. Phys.* **1994**, *101*, 9663.
(4) Liu, L.; Guo, H. *Chem. Phys. Lett.* **1995**, *237*, 299.
(5) Michl, J.; Bonačić-Koutecký, V.; *Electronic aspects of organic photochemistry*; Wiley: New York, 1990.
(6) Stock, G.; Domcke, W. *J. Phys. Chem.* **1993**, *97*, 12466.
(7) Dixon, R. N. *Chem. Soc. Rev.* **1994**, 375,
(8) Klessinger, M. *Angew. Chem., Int. Ed. Engl.* **1995**, *34*, 549.
(9) Clifford, S.; Bearpark, M. J.; Bernardi, F.; Olivucci, M.; Robb, M. A.; Smith, B. R. *J. Am. Chem. Soc.* **1996**, *118*, 7353.
(10) Sension, R. J.; Repinek, S. T.; Hochstrasser, R. M. *J. Chem. Phys.* **1990**, *93*, 9185.
(11) Seidner, L.; Stock, G.; Domcke, W. *J. Chem. Phys.* **1995**, *103*, 3998.
(12) Stock, G. *J. Chem. Phys.* **1995**, *103*, 10015.
(13) Hynes, J. T.; Kapral, R.; Torre, G. M. *J. Chem. Phys.* **1980**, *72*, 177.
(14) Rejto, P. A.; Bindewald, E.; Chandler, D. *Nature* **1995**, *375*, 129.
(15) Sakka, T.; Matsumara, K.; Tsuboi, T.; Ogata, Y. H. *Chem. Phys. Lett.* **1998**, *286*, 107.
(16) Pacher, T.; Cederbaum, L. S.; Köppel, H. *Adv. Chem. Phys.* **1993**, *84*, 293.
(17) Persico, M. In *Encyclopedia of Computational Chemistry*; Schleyer, P. v. R., Allinger, N. L., Clark, T., Gasteiger, J., Kollman, P. A., Schaefer, III, H. F., Schreiner, P. R., Eds.; Wiley: Chichester, UK, 1998; p 852.
(18) Persico, M. In *Spectral Line Shapes*; Rostas, F., Ed.; De Gruyter: Berlin, 1985, Vol. 3, p 587.
(19) Cimiraglia, R.; Malrieu, J.-P.; Persico, M.; Spiegelmann, F. *J. Phys. B* **1985**, *18*, 3073.
(20) Cattaneo, P.; Persico, M. *Chem. Phys.* **1997**, *214*, 49.
(21) Cattaneo, P.; Persico, M.; Tani, A., to be published.
(22) Tully, J. C. *J. Chem. Phys.* **1990**, *93*, 1061.
(23) Tully, J. C. *Int. J. Quantum Chem. Symp.* **1991**, *25*, 299.
(24) Ferretti, A.; Granucci, G.; Lami, A.; Persico, M.; Villani, G. *J. Chem. Phys.* **1996**, *104*, 5517.
(25) Cattaneo, P.; Persico, M. *J. Phys. Chem. A* **1997**, *101*, 3454.
(26) van Gunsteren, W. F.; Berendsen, H. J. C. *Mol. Phys.* **1982**, *45*, 637.
(27) Hase, W. L.; Duchovic, R. J.; Hu, X.; Lim, K. F.; Lu, D.-H.; Peslherbe, G. H.; Swamy, K. N.; Vande Linde, S. R.; Wang, H.; Wolf, R. J. *Quantum Chemistry Program Exchange* **1996**, *16*, 671.
(28) Harris, A. L.; Brown, J. K.; Harris, C. B. *Annu. Rev. Phys. Chem.* **1988**, *39*, 341.
(29) Brown, J. K.; Russell, D. J.; Smith, D. E.; Harris, C. B. *Rev. Phys. Appl.* **1987**, *22*, 1787.
(30) Fogel, L. D. J.; Steel, C. *J. Phys. Chem.* **1976**, *98*, 4859.
(31) Burton, K. A.; Weisman, R. B. *J. Am. Chem. Soc.* **1990**, *112*, 1804.
(32) Andrews, B. K.; Burton, K. A.; Weisman, R. B. *J. Chem. Phys.* **1992**, *96*, 1111.
(33) North, S. W.; Longfellow, C. A.; Lee, Y. T. *J. Chem. Phys.* **1993**, *99*, 4423.
(34) Fairbrother, D. H.; Dickens, K. A.; Stair, P. C.; Weitz, E. *Chem. Phys. Lett.* **1995**, *246*, 513.
(35) Cattaneo, P.; Persico, M. *Chem. Phys. Lett.* **1998**, *289*, 160.
(36) Cattaneo, P.; Persico, M., to be published.
(37) Engel, P. S., *Chem. Rev.* **1980**, *80*, 99.
(38) Cattaneo, P.; Persico, M. *Theoret. Chem. Acc.*, accepted.
(39) FORTRAN subprograms and parameters of the PES and couplings may be requested from M. Persico: e-mail mau@hermes.dcci.unipi.it.
(40) Liu, R.; Cui, Q.; Dunn, K. M.; Morokuma, K. *J. Chem. Phys.* **1996**, *105*, 2333.
(41) Landolt-Börnstein *Numerical data and functional relationships in Science and Technology*; VI ed., vol. II/5a, 1969.
(42) Cattaneo, P.; Persico, M., to be published.
(43) Dubs, M.; Brühlmann, U.; Huber, J. R. *J. Chem. Phys.* **1986**, *84*, 3106.
(44) Lavi, R.; Bar, I.; Rosenwacs, S. *J. Chem. Phys.* **1987**, *86*, 1639.
(45) Cimiraglia, R.; Persico, M.; Tomasi, J. *J. Am. Chem. Soc.* **1985**, *107*, 1617.
(46) Persico, M.; Cacelli, I.; Ferretti, A. *J. Chem. Phys.* **1991**, *94*, 5508.
(47) Lenderink, E.; Wiersma, D. A. *Chem. Phys. Lett.* **1994**, *218*, 586.
(48) Chow, Y. L. *The chemistry of amino, nitro and nitrosocompounds and their derivatives*; Patai, S., Ed.; Wiley: New York; 1982; p 181.
(49) Adeleke, B. B.; Wan, J. K. S. *Mol. Photochem.* **1974**, *6*, 329.
(50) Huron, B.; Malrieu, J.-P.; Rancurel, P. *J. Chem. Phys.* **1973**, *58*, 5745.
(51) Cimiraglia, R.; Persico, M. *J. Comput. Chem.* **1987**, *8*, 39.
(52) Bouteiller, Y.; Mijoule, C.; Nizam, M.; Barthelat, J. C.; Daudey, J. P.; Pelissier, M.; Silvi, B. *Mol. Phys.* **1988**, *65*, 295.
(53) Tomasi, J.; Persico, M. *Chem. Rev.* **1994** *94*, 2027.